Short Communication

Structural and Morphological Properties of MnO₂/MWCNT Composite Grown Using the Hydrothermal Method for Supercapacitor Application

Agus Subagio[1,], Yusro Al Hakim[2], Mohamad Wahyu Ristiawan[1], Muhammad Abdul Kholil[1], Priyono[1]*

[1] Department of Physics, Faculty of Science and Mathematics, Diponegoro University, Jl. Prof. Sudarto, SH, Tembalang, Semarang 50275, Indonesia
[2] Department of Physics Education, Purworejo Muhammadiyah University, Jl. KH. Ahmad Dahlan 3 & 6 Purworejo 54111, Indonesia
[*]E-mail: agus_fadhil@yahoo.com

Manganese dioxide and multi-walled carbon nanotubes (MWCNT) have received considerable recent interest for their potential application in supercapacitors, MnO_2 as a pseudocapacitor material and MWCNT as an electrochemical double layer capacitance (EDLC) material. The combination of MnO_2 and MWCNT is expected to make promising supercapacitor electrodes. In this study, MnO_2 was mixed with MWCNT during the hydrothermal process. The difficulty in obtaining MnO_2/MWCNT composite homogeneity in the hydrothermal process provides a challenge to scaling up production. $KMnO_4$ and MWCNT were mixed with 20 mL distilled water and stirred using a magnetic stirrer for 2 minutes, then placed into an autoclave. Heating of autoclave was carried out at 160°C for 3 hours in an oven and followed by cooling at room temperature naturally. Manganese dioxide/MWCNT composites were made in 1:1 and 3:1 ratios. The diffraction peaks of composites indicated that incorporation of MWCNT into MnO_2 has provided a crystalline orientation derived from MnO_2 and MWCNT. Scanning electron microscopy and TEM imaging demonstrated that MnO_2/MWCNT 3:1 composite attained better homogeneity than MnO_2/MWCNT 1:1 as indicated by the attachment of MnO_2 to the entire nanotubes surface of MWCNT. Increasing of conductivity values have been supported by MWCNT marked decreasing in the R_{ct} value in electrochemical impedence spectroscopy measurements. Based on cyclic voltammogram measurements, the MnO_2/MWCNT electrode 3:1 produced specific capacitation (C_s) of 252 F/g with stability up to 1000 cycles.

Keywords: MWCNT, MnO₂, hydrothermal method, structural, morphology, supercapacitor

1. INTRODUCTION

To date, many materials have been studied as supercapacitor electrodes such as manganese dioxide (MnO₂), nickel oxide/hydroxide, cobalt oxide/hydroxide and conducting polymer. In recent

years, manganese oxide has garnered increasing attention for its potential use in energy storage media, catalysis, ion transport, molecular adsorption and biosensors due to its unique physical and chemical properties [1-11]. As an energy storage material, manganese oxide is especially important because of its high capacitance capability, abundance in nature, very low inherent toxicity, potential produced (approaching one volt) is large enough to trigger high energy storage, environmentally friendliness and low cost.

Manganese dioxide has a layered or tunnel-shaped crystal structure that can facilitate the diffusion of ions into bulk material. It has very low electrical conductivity (10^{-4}-10^{-6} S.cm^{-1}) by itself however, which can be increased by combining it with multiwalled carbon nanotubes (MWCNT) that have high electrical conductivity and mechanical strength [12]. In general, supercapacitors can provide higher power than most batteries because a large amount of charge can be stored in a double layer. But for power density relatively low, because of series resistance of two electrodes. Increasing power and power density requires material with high capacitance and low resistance. Manganese dioxide combined with MWCNT should optimize the performance of supercapacitors as MWCNT will provide percolation of the active particles more efficiently compared to traditional carbon materials and form the open mesopore network that drives the ion diffusion to the composites' active surface [13].

Manganese dioxide has been synthesized in a number of ways, including by thermal decomposition [13], the sol-gel process [14], refluxing [15], sonochemical reduction [16] and hydrothermal [17]. The hydrothermal method is the preferred method because it can produce multiple shapes with a simple process [18]. Other advantages include energy savings (carried out at low temperatures), cost-effectiveness, simplicity, high purity (conducted within tightly-closed containers), high reaction rates and low temperatures when using the right solvent [19]. In previous studies, the synthesis between MnO_2 and MWCNT was carried out separately so that the incorporation of MnO_2 and MWCNT materials became less than perfect. This causes low homogeneity and restricts transfer of redox reaction charges. In addition, the composition between MnO_2 and MWCNT under *in-situ* hydrothermal process also affects homogeneity of composite. High homogeneity of MnO_2/MWCNT composites will decrease composite agglomeration. Charge transfer is mediated by the high conductivity of MWCNT, so that the homogeneity of composites achieved with the hydrothermal method is advantageous to scaling up. This necessitates appropriate composition adjustment between MnO_2 and MWCNT under *in-situ* hydrothermal conditions.

In this study, MnO_2/MWCNT was synthesized using the hydrothermal method. Multi-walled carbon nanotubes were mixed with MnO_2 in certain ratios and subjected to an *in-situ* hydrothermal process so that the composite of materials maximized homogeneity. The incorporation of MWCNT and MnO_2 can make promising supercapacitor electrodes.

2. EXPERIMENTAL

2.1. Preparation of MnO₂/MWCNT composites.

Synthesis of MnO_2 was carried out in a 20 ml Teflon-lined stainless-steel autoclave [18]. MnO_2 nanorods were synthesized using 2.5 mmol $KMnO_4$ dissolved in distilled water at room temperature. Hydrochloric acid was added and the solution was stirred for ten minutes using a magnetic stirrer then placed into an autoclave (20 ml). Separately, MWCNT were synthesised using the spray pyrolysis

method. Three g of ferrocence and 50 ml benzene were combined and stirred using a magnetic sterilizer for 30 minutes, and the solution injected into a tube heated at 900°C and flooded with argon gas for 30 minutes. After cooling to room temperature [20], the product was refluxed using 65% HNO_3, cured with distilled water to neutral pH and dried to produce MWCNT [21].

Multi-walled carbon nanotubes and $KMnO_4$ were combined using the hydrothermal process. After mixing with 20 mL distilled water and stirred using a magnetic stirrer for 2 minutes, the MWCNT and $KMnO_4$ solution was placed into an autoclave. The autoclave was heated in oven mode at 160 °C for 3 hours then cooled to room temperature. Four samples were used in this study MWCNT powder, MnO_2 powder, MnO_2/MWCNT 1:1 and MnO_2/MWCNT 3:1.

2.2. Structure characterization

The intensity and angle of x-ray scattering of the material was obtained using X-ray diffraction spectroscopy (XRD, Philip Analytical X-Ray) with CuKα radiation (λ=1.5418 Å) at 40 kV and 20 mA adjusted to the MnO_2/MWCNT crystal structure database. Morphology of samples was characterized using a scanning electron microscope (SEM, JEOL-6510LA) and transmission electron microscope (TEM). The FTIR spectra were obtained using a Nicolet Avatar 360 FTIR spectrometer.

2.3. Electrochemical measurement

To fabricate supercapacitor electrodes, 0.2 g of ethylcellulose was dissolved in 4 mL ethanol and the solution stirred for 10 minutes, followed by mixing 1.6 g terpineol into the binder. The MnO_2/MWCNT was dispersed in the binder by stirring for 10 minutes. Then MnO_2/MWCNT paste was deposited onto the SS foil substrate by using the doctor blade method and drying at 150 °C for 2 hours. Electrochemical impedance spectroscopy (EIS) and cyclic voltametry (CV) measurements performed using LCR meter HIOKI 3532-50 chemical impedance meter and WBCS3000S Wonatech, respectively. The measurements were carried out in a standard double cell containing 1 M KCl aqueous solution.

3. RESULTS AND DISCUSSION

As the hydrothermal process synthesis of MnO_2/MWCNT was carried out within a closed container, the ideal gas laws were applicable. In the ideal gas law, there are three related quantities: pressure, temperature and volume. In the hydrothermal method, the volume of gas in a closed space is fixed [22]. The formation of MnO_2 from the hydrothermal process using $KMnO_4$ and HCl in the form of a $KMnO_4$ reduction reaction can be written [23]:

$$2KMnO_4 + 8HCl \rightarrow 2MnO_2 + 3Cl_2 + 4H_2O + 2KCl$$

The reaction also reflects the nucleation or growth process of MnO_2. After heating to a sufficiently high temperature (>140°C), $KMnO_4$ atoms become active, forming the MnO_2 nucleus by decomposition in HCl and water [24]. After that, the growth process of MnO_2 is strongly influenced by the environment, affecting the shape and aggregation of particles. The number of MnO_2 nuclei at the initial nucleation stage and the crystal growth process is influenced by $KMnO_4$ concentration [25]. Thus, the MnO_2 nanostructure is very much determined by the concentration of $KMnO_4$ during synthesis. In

the hydrothermal process, MWCNT does not react with $KMnO_4$ and HCl. The hydrothermal method can help increase crystallinity in materials through the influence of temperature and reaction time [26]. X-ray diffraction spectroscopy characterization was used to determine the crystallinity level of MWCNT and MnO_2. Characterization of XRD-synthesized compounds was performed using instruments with an angle range of $2\theta = 10\text{-}90°$ and wavelength of 1.5418Å. The test was carried out on a synthesis sample based on the difference in the MWCNT and MnO_2 mass ratios in the hydrothermal process. The XRD test results were analyzed by Match! Program using Crystallography Open Database (COD) and based on references in previous studies.

Figure 1a shows that the formed MWCNT has a graphene type carbon structure, based on standard powder diffraction data and previous studies conducted by Hashemzadeh, et.al. (2009) [14]. Presence of graphene shown at peak 2θ of 26.3° and 43.9° is at the angle of 2θ formed C (002). The synthesized XRD pattern of MnO_2 can be seen in Figure 1b. The diffraction pattern shows a peak at 2θ of 12.9°, 24.2°, 37.8°, 60.5° and 66.2° with the Miller index of (110), (131), (200), (411) and (231) with the index representing a reflection of the plane of the phase α-MnO_2. The peak of 40.9° with Miller index of (400) representing the phase β-MnO_2 in accordance with COD databases No.96-151-4235, 96-151-4117, 96-810-3499 and 96-151-4108 [16]. The diffraction peaks of MnO_2/MWCNT 3:1 composite compared with those of MnO_2/MWCNT 1:1 composite showed that the crystallinity of MWCNT increased with increasing MWCNT mass.
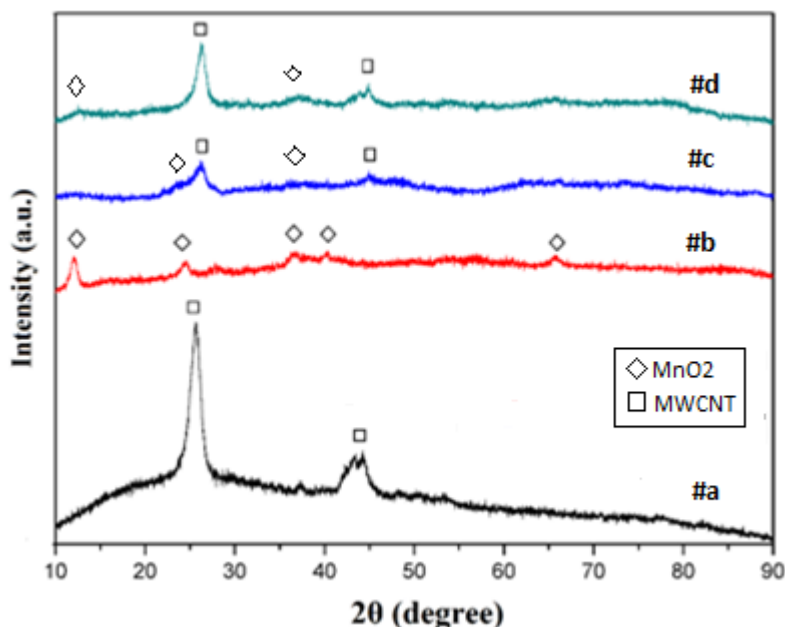

Figure 1. XRD image of a) MWCNT; b) MnO_2; c) MnO_2/MWCNT 3:1 and d) MnO_2/MWCNT 1:1

The morphology of MWCNT, MnO_2, and MnO_2/MWCNT with mass ratio 1:1 and 3:1 was determined using the SEM image as shown in Figure 2. Figure 2(a) shows the morphology of MnO_2 nanorods which coagulate to form nanoflowers (such as flowers). Figures 2(b) and 2(c) show the morphology of MnO_2/MWCNT nanorods with a combination of MnO_2.

The result of MnO_2/MWCNT synthesis by the hydrothermal method shows the results of even mixing. During the $KMnO_4$ reduction process, crystals grown from MnO_2 condense into two-dimensional (2D) MnO_2 sheets. Then, at high temperatures and pressures under hydrothermal

conditions, MnO_2 forms small nanorods. Morphology of one-dimensional MnO_2 such as nanotubes, nanowires and nanorods has more advantages compared to other structures, such as short ion diffusion paths and continuous electron transport pathways. Nanorod morphology provides a high surface area to volume ratio which increases material sensitivity, ion diffusion ability and specific capacitance values. Smaller nanorods grow to be bigger and more stable [23]. Stability in the morphology of nanorods also results in oriented attachments to MnO_2 material which can produce morphology of nanorods with aggregation.
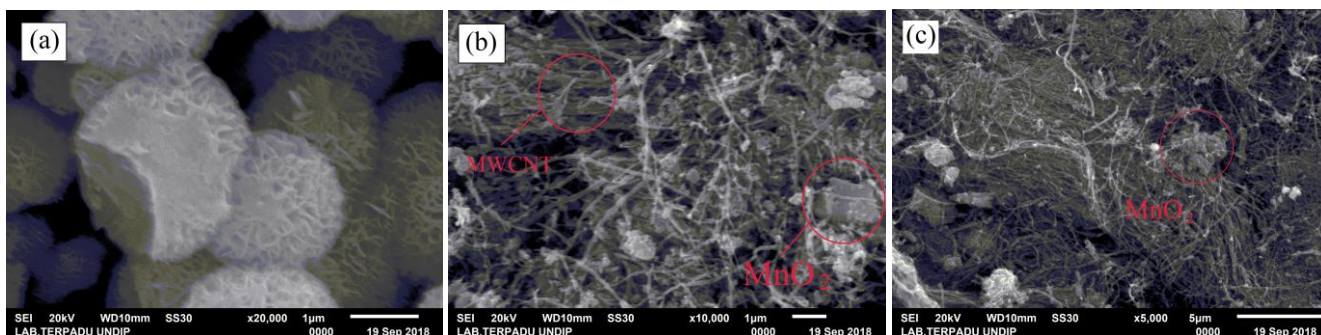

Figure 2. SEM images of (a) MnO_2, (b) $MnO_2/MWCNT$ 1:1, (c) $MnO_2/MWCNT$ 3:1.

Manganese dioxide morphology was further characterized by transmission electron microscopy (TEM). The results of this analysis showed morphological and distribution images in the sample. The TEM results shown in Figure 3 indicate that MnO_2 material sticks to the wall of MWCNT due to the hydrothermal method. The MWCNT tube size was approximately 40 nm. In the $MnO_2/MWCNT$ 1:1 sample the surface of the nanotubes were not evenly coated by MnO_2, whereas in the $MnO_2/MWCNT$ 3:1 sample MnO_2 could coat all surfaces of the nanotubes. The homogeneity of MnO_2 coating on the MWCNT surface will greatly affect the capacitor performance of the composite. The addition of a larger MnO_2 composition allows the MnO_2 coating process on the surface of the nanotube to be more thorough during the hydrothermal process.
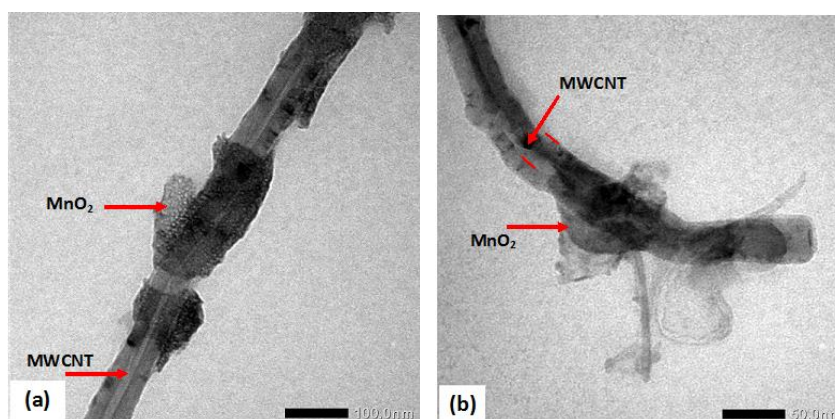

Figure 3. TEM image of (a) $MnO_2/MWCNT$ 1:1 and (b) $MnO_2/MWCNT$ 3:1

The FTIR spectra of MWCNT, $MnO_2/MWCNT$ 3:1, $MnO_2/MWCNT$ 1:1 and MnO_2 are shown in Figure 4. FTIR spectra were recorded in the range of 4000-500 cm^{-1} in transmittance mode. The peak

near 3400 cm^{-1} is attributed to the vibration of the free or bonded OH/COOH groups. This peak could be allocated to the -OH group of the carboxylic groups attached with MnO$_2$/MWCNT. The peak around 1430 cm^{-1} was attributed to C-O vibrations from epoxy groups. The peak at 1429 cm^{-1} was due to the Mn-OH deformation vibration. The peaks located at 1513 cm^{-1} and 1322 cm^{-1} were attributed to the C=C and C=C stretching. The peak located at 1200 cm^{-1}, originated from the stretching vibration of C-O-C bond. The peak at 553 cm^{-1} was attributed to the Mn-O stretching vibration, indicating the presence of the MnO$_2$ crystal, evidence of successful MnO$_2$ deposition. The FTIR results indicated the creation of the composites of MWCNT and MnO$_2$. The major groups such as -OH, -COOH, -C=C, -C-O, Mn-OH and Mn-O appeared on the surface of MnO$_2$/MWCNT composite. These results are consistent with that in other works [27-30].

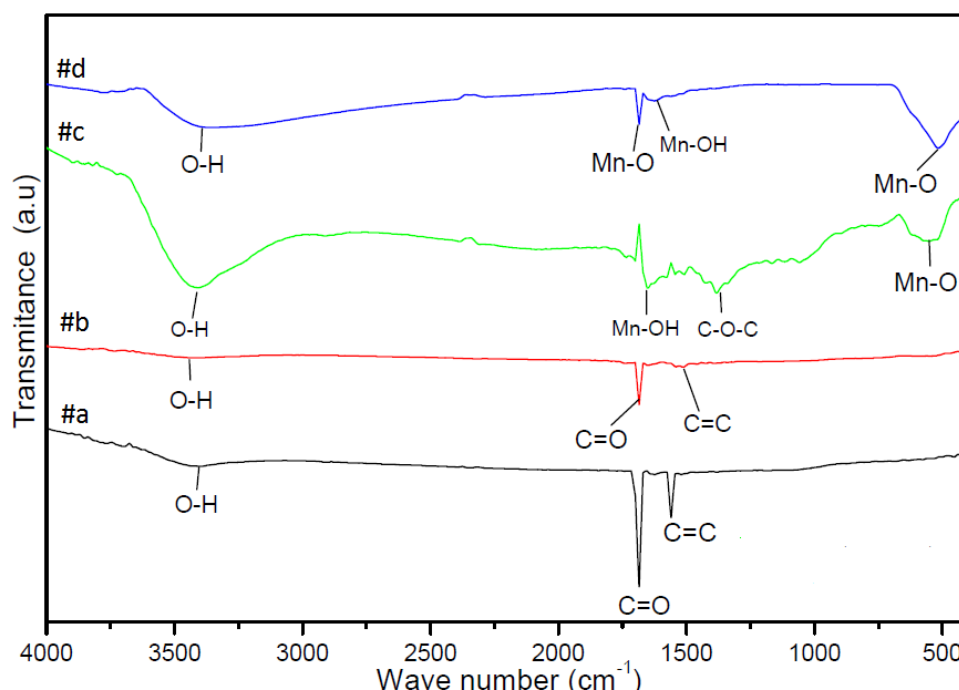**Figure 4.** FTIR spectra of a) MWCNT; b) MnO$_2$/MWCNT 1:1; c) MnO$_2$/MWCNT 3:1 and d) MnO$_2$

Electrochemical impedance spectroscopy measurements were carried out in the frequency range from 100 kHz to 10 mHz in order to evaluate the frequency response of MnO$_2$, MWCNT and MnO$_2$/MWCNT electrodes. These measurements were useful in evaluating the resistive factor of the electrode and characterization of EIS was conducted to understand the interaction between electrolyte and electrode. Figure 5 represents the Nyquist plot of supercapacitor of MnO$_2$/MWCNT electrodes to obtain the circuit resistance (R_{ct}) of the electrode by measuring the semicircular diameter on the real axis. This resistance corresponds to the resistance at the electrolyte/electrode interface [31]. The magnitude of R_{ct} obtained from the semicircle loop of the Nyquist plot were found to be 28 Ω, 412 Ω, 1512 Ω and 2418 Ω for MnO$_2$/MWCNT 3:1, MnO$_2$/MWCNT 1:1, MWCNT and MnO$_2$, respectively. Manganese dioxide/MWCNT samples had smaller R_{ct} values than others indicating that the load transfer process was well-mediated in the presence of MWCNT which increases the material conductivity value. The R_{ct} value for MnO$_2$/MWCNT 3:1 was greatly improved after the incorporation of MWCNT to

MnO_2. However, the MWCNT electrode still had relatively high R_{ct} due to the presence of an ion diffusion mechanism which should be mediated by oxide material (in this case MnO_2).
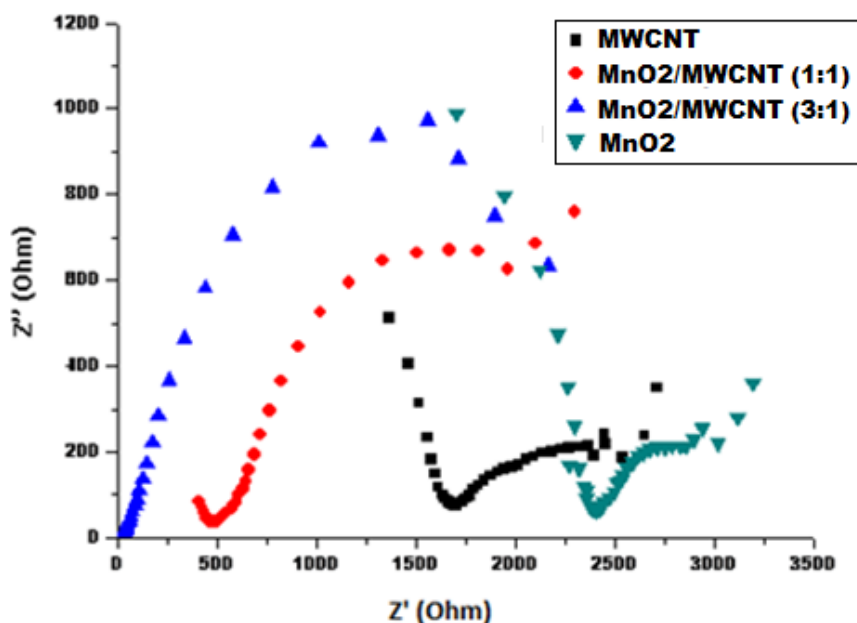

Figure 5. Nyquist plots of the EIS of MWCNT, MnO_2/MWCNT 1:1, MnO_2/MWCNT 3:1 and MnO_2.

Cyclic voltammetry testing was carried out using a WBCS3000 tool, Automatic Battery Cycler Ver.3.2. The purpose of cyclic voltammetry testing was to determine the capacitive properties of MnO_2/MWCNT 1:1 and MnO_2/MWCNT 3:1 electrodes in 1 M KCl aqueous solution. Data obtained from testing cyclic voltammetry in the form of a potential curve to the current. The measurement of the specific capacitance values was with variations in scan rates of 200, 150, 100, 50 and 25 mV/s. The curve pattern formed a hysteresis curve with quasi square or rectangular shapes. The hysteresis pattern showed that the supercapacitor electrodes used have capacitive properties, i.e, when the voltage reaches 0.4 volts and is reduced to -0.4 volts, the current value produced does not have the same current value as before.

Figure 6 shows cyclic voltammograms of (a) MnO_2/MWCNT 1:1 and (b) MnO_2/MWCNT 3:1 electrode material at scan rates from 25 mV/s to 200 mV/s. The ion diffusion process at a low scan rate is lengthy. Ions and electrons coming from the current collector will diffuse evenly to the electrode surface to the pore meso depending on the homogeneity of MnO_2/MWCNT. Increasing the homogeneity of MnO_2/MWCNT through the hydrothermal process will support this diffusion process. An increase in the width of the charge current and discharge curve will occur, indicated by a large capacitance value. On the other hand, at a high rate of induction, the ion diffuses rapidly but only just reaches the surface of the electrode, resulting in a small charge and discharge current curve which indicates a low capacitance value.
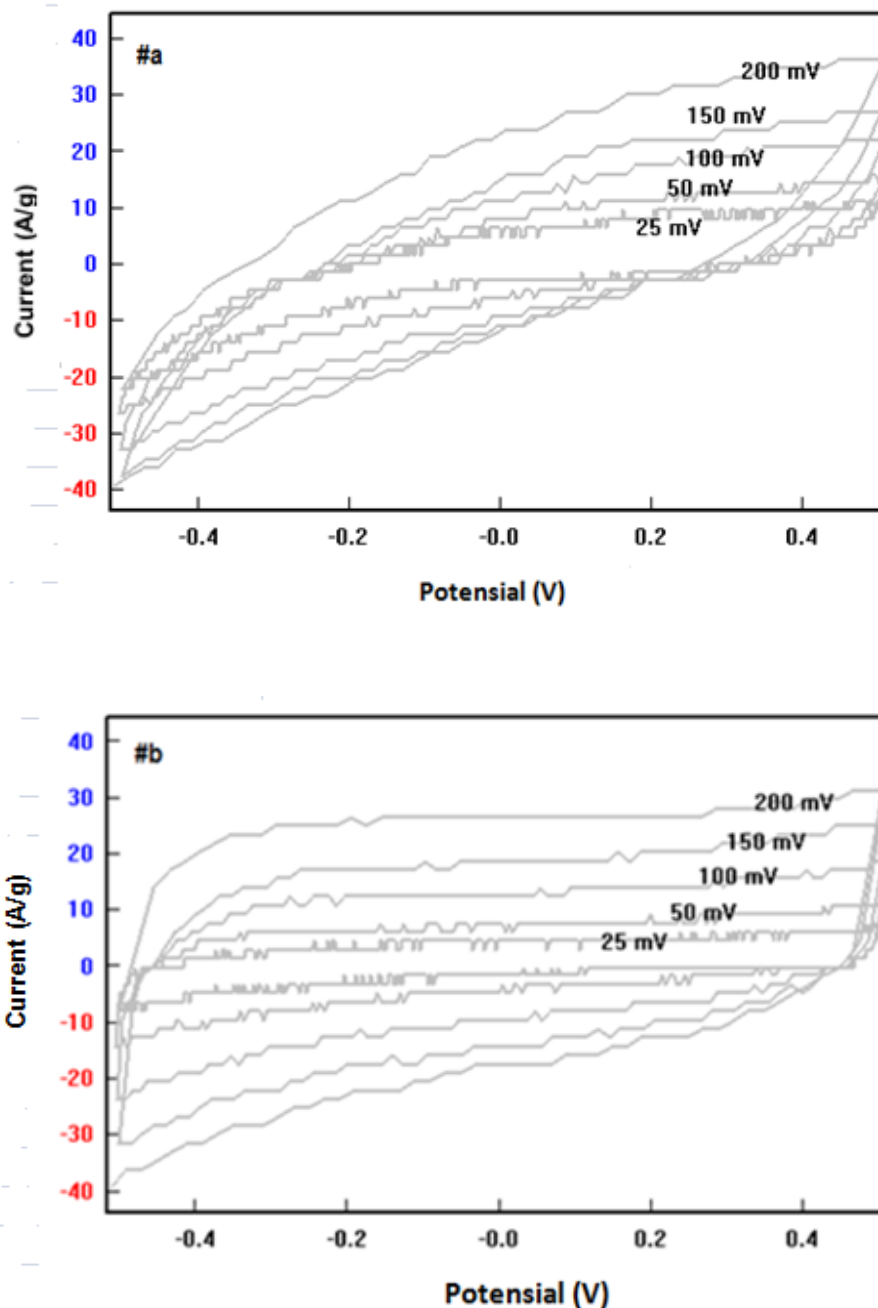
Figure 6. Cyclic voltammograms of (a) MnO$_2$/MWCNT 1:1 and (b) MnO$_2$/MWCNT 3:1 electrode material at scan rates from 25 mV/s to 200 mV/s.

The galvanostatic charging/discharging curves of the composites electrodes at a current density of 0.5, 1.0 and 2.0 A/g are shown in figure 7. The sample MnO$_2$/MWCNT 3:1 in figure 7b shows the charging/discharging curves have more symmetrical properties than sample MnO$_2$/MWCNT 1:1 in figure 7a. This shows that the sample MnO$_2$/MWCNT 3:1 has good electrochemical capacitive characteristics and superior reversible Faradaic reactions, implying excellent reversibility and high coulombic efficiency. The specific capacitance can be calculated from the discharging curve based on the equation [32,33,34]:

$$C_s = \frac{I.\Delta t}{m.\Delta V}$$

Here I (A) is the applied current, Δt (s) is the discharge time, m (g) is the mass of active material, ΔV (V) is the discharging potential window.

In the curve produced a specific capacitance value calculated at 0.5 A/g for the sample MnO_2/MWCNT 3:1 of 252 F/g and this value was greater than the sample MnO_2/MWCNT 1:1 of 170 F/g. This shows that the homogeneity of the sample MnO_2/MWCNT 3:1 was better than that of MnO_2/MWCNT 1:1 because MnO_2 can fully coat the surface of the nanotube of MWCNT as shown in TEM images.
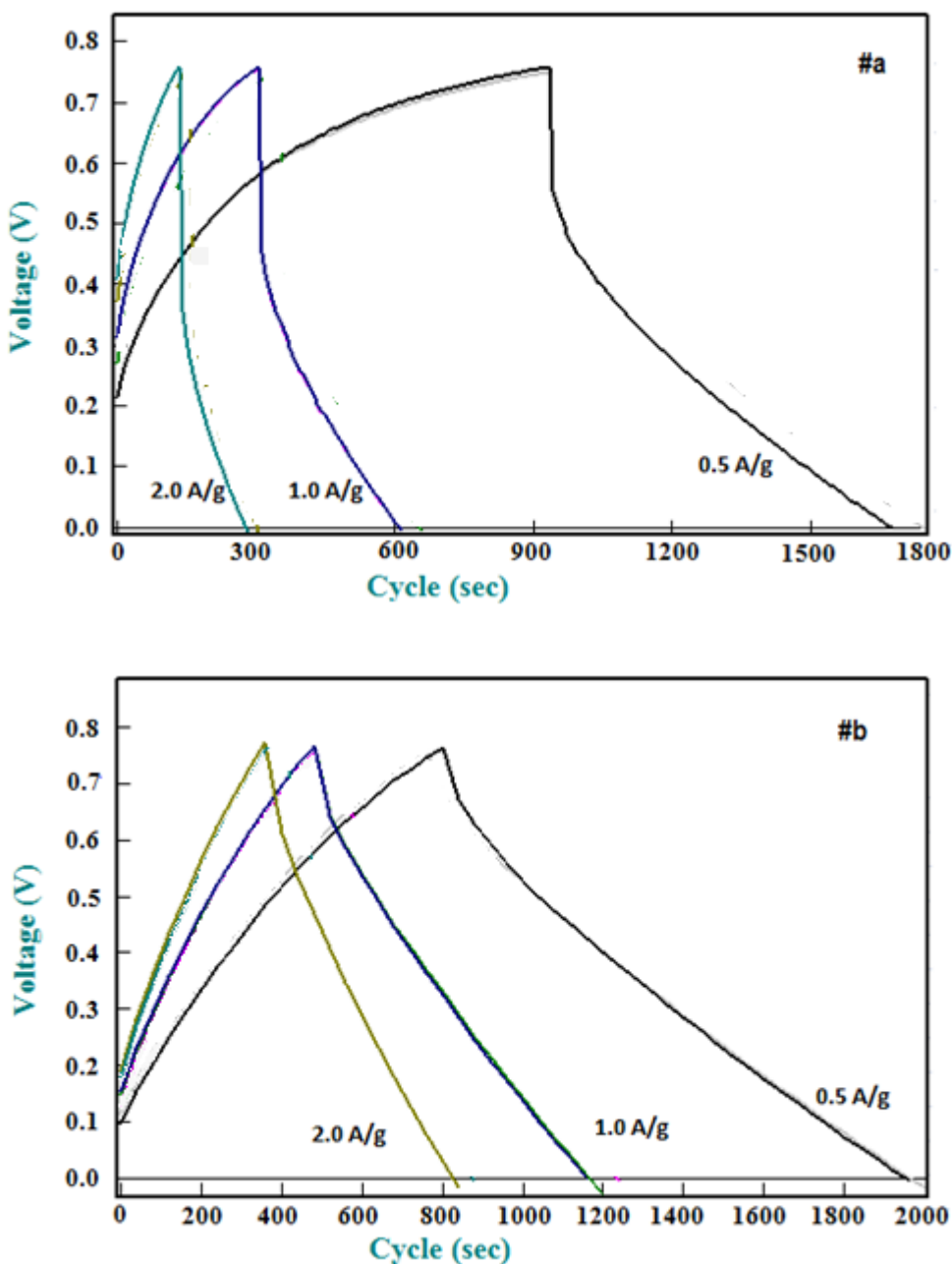

Figure 7. The galvanostatic charging/discharging curves at current density of 0.5, 1.0 and 2.0 A/g of (a) MnO_2/MWCNT 1:1 and (b) MnO_2/MWCNT 3:1 electrodes.

Figure 8 shows the variation of specific capacitance (C_s) with cycle numbers of charge–discharge at a constant current density of 0.5 A/g based on the calculation of above equation. The change of C_s with the increase in deposition time was consistent with CV analysis. The MnO_2/MWCNT 3:1 electrode achieved the highest C_s of 252 F/g. After 1000 cycles of testing, its C_s remained at 245 F/g, about 97% of the initial value, though electrolyte is used. It indicates that the MnO_2/MWCNT 3:1 electrode process good reversibility in the repetitive charge/discharge cycling and showed their potential in the application of supercapacitors. Conversely, there was instability in the MnO_2/MWCNT electrode 1:1 with a C_s starting at 120 F/g that increased to around 160 F/g at 200 cycles and then reaching 170 F/g at the end of the 1000 cycles.
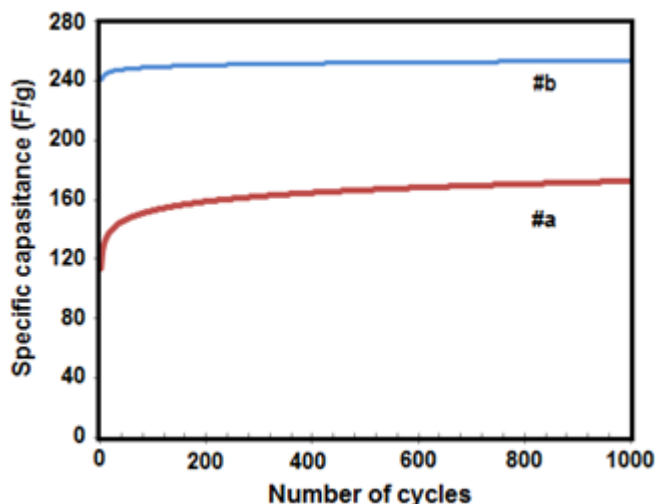

Figure 8. The specific capacitance (C_s) of (a) MnO_2/MWCNT 1:1 and (b) MnO_2/MWCNT 3:1 electrodes is as a function of number of cycles at a constant current density of 0.5 A/g.

Figure 9 shows Coulombic efficiency remained at an average 95% after the 920 cycles indicating the remarkable long-term stability of the MnO_2/MWCNT 3:1 electrode. It also indicates the excellent charge-discharge reversibility of the electrode and potential for supercapacitor application.
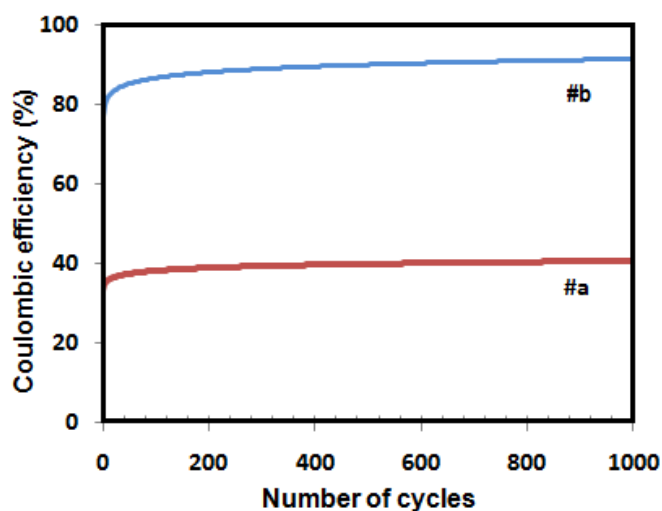

Figure 9. Variation of the Coulombic efficiency of (a) MnO_2/MWCNT 1:1 and (b) MnO_2/MWCNT 3:1 electrodes as a function of number of cycles at a constant current density of 0.5 A/g.

Table 1 shows the specific capacitance values of the MnO_2/MWCNT electrodes obtained from other methods. It can be seen that the results of the research that we did produce relatively high C_s values

Table 1. MnO_2/MWCNT specific capacitance (C_s) of several methods.

Samples	Method	Electrolite	Specific Capacitance (C_s) F/g	Ref.
MnO_2/MWCNT 3:1	hydrothermal	KCl	252	This study
CNT@NCT@MnO_2 3D	chemical method	Na_2SO_4	210	[1]
CNT-MnO_2 nanoflaky	chemical method	Na_2SO_4	145.6	[10]
MWCNT/MnO_2	sonochemical	Na_2SO_4	394	[16]
3D MnO_2–CNT	in-situ hydrothermal	Na_2SO_4	214	[26]
MnO_2/rGO-CNT	modified hummers	KCl	295.83	[28]
MnO_2@NCNTs@MnO_2	solvothermal	Na_2SO_4	253.1	[30]

4. CONCLUSION

In conclusion, this results show that successful synthesis of MnO_2/MWCNT can explain incorporation of MWCNT into MnO_2 using the hydrothermal method. The diffraction peaks of MnO_2/MWCNT 1:1 and MnO_2/MWCNT 3:1 showed that the crystallinity of MWCNT increased with increasing MWCNT mass. Both TEM images of MnO_2/MWCNT 1:1 and 3:1 composites showed that MnO_2 material was attached to MWCNT walls by the hydrothermal process, and MnO_2/MWCNT 3:1 allowed for MnO_2 to cover all surfaces of MWCNT. This demonstrated better homogeneity so that the specific capacitance (C_s) of 252 F/g was produced with stability up to 1000 cycles.

References

1. Y. Wang, D. Zhang, Y. Lu, W. Wang, T. Peng, Y. Zhang, Y. Guo, Y. Wang, K. Huo, J. K. Kim and Y. Luo, *Carbon*, 143 (2019) 335.
2. Q. Yua, C. Wanga, X. Lia, Z. Lia, L. Wanga, Q. Zhanga, G. Wua and Z. Li, *Fuel*, 239 (2019) 1240.
3. J. Jia, R. Ran, X. Guo, X. Wu, W. Chen and D. Weng, *Catal. Commun.*, 119 (2019) 139.
4. Y. Wei, L. Ni, M. Li and J. Zhao, *Catal Today*, 297 (2017) 188.
5. Y. Zhang, F. Wang, P. Ou, H. Zhu, Y. Lai, Y. Zhao, W. Shi, Z. Chen, S. Li and T. Wang, *J. Hazard. Mater.*, 360 (2018) 223.
6. M. Ghejua, I. Balcu and G. Mosoarca, *J. Hazard. Mater.*, 310 (2016) 270.
7. M. Seredych and T. J. Bandosz, *Microporous Mesoporous Mater.*, 150 (2012) 55.
8. K. Vijayalakshmi, A. Renitta, K. Alagusundaram and A. Monamary, *Mater. Chem. Phys.*, 214 (2018) 431.
9. H. L. Xu and W.D. Zhang, *Chin. Chem. Lett.*, 28 (2017) 143.

10. D. Ganguly, D. Pahari, N. S. Das, P. Howli, B. Das, D. Banerjee and K. K. Chattopadhyay, *J. Electroanal. Chem*., 778 (2016) 12.
11. A. Subagio, Priyono, Pardoyo, Aswardi, R. Yudianti, A. Subhan and E. Taer, *Mater. Sci. Forum,* 827 (2015) 113.
12. D. Z. W. Tan, H. Cheng, S. T. Nguyen and H. M. Duong, *Mater. Technol. Adv. Func. Mater.*, 29 (2014) 107.
13. S. H. Kim, S. J. Kim and S. M. Oh, *Chem. Mater.*, 11 (1999) 557.
13. H. Pan, J. Li and Y. P. Feng, *Nanoscale Res. Lett.*, 5 (2010) 654.
14. F. Hashemzadeh, M. M. K. Motlagh and A. Maghsoudipour, *J. Solgel Sci. Technol.*, 51 (2009) 169.
15. X. M. Liu and S. Y. Fu, *Powder Technol.*, 154 (2005) 120.
16. H. R. Naderi, M. R. Ganjali and P. Norouzi, *Int. J. Electrochem. Sc.,* 11 (2016) 4267.
17. N. Li, X. Zhu, C. Zhang, L. Lai, R. Jiang and J. Zhu, *J. Alloys Compd*, 692 (2017) 26.
18. D. Q. A'Yuni, I. Alkian, F. K. Sya'Diyah, Kadarisman, A. Darari, V. Gunawan and A. Subagio, *J. Phys. Conf. Ser.*, 909 (2017) 012004.
19. M. W. Ristiawan, Priyono, A. Subagio, M. A. Kholil and A. Ajiesastra, *J. Phys. Sci.*, 29 (2018) 257.
20. A. Darari, H. R. Ardiansah, A. Arifin, N. Rismaningsih, A. N. Ningrum and A. Subagio, *AIP Conf. Proc.*, 1725 (2016) 020012.
21. S. A. Wulandari, A. Arifin, H. Widiyandari and A. Subagio, *J. Phys. Conf. Series*, 1025 (2018) 012005.
22. L. E. Greene, B. D. Yuhas, M. Law, D. Zitoun and P. Yang, *Inorg. Chem.*, 45 (2006) 7535.
23. S. K. Meher and G. R. Rao, *The J. Phys. Chem.,* 117 (2013) 4888.
24. X. Duan, J. Yang, H. Gao, J. Ma, L. Jiao and W. Zheng, *Cryst. Eng. Comm*., 14 (2012) 4196.
25. L. Feng, Z. Xuan, H. Zhao, Y. Bai, J. Guo, C. W. Su and X. Chen, *Nanoscale Res. Lett.*, 9 (2014) 290.
26. F. Teng, S. Santhanagopalan, Y. Wang and D. D. Meng, *J. Alloys Compd*, 499 (2010) 259.
27. Y. Chen, L. Chen, P. Li, Y. Xu, M. Fan, S. Zhu and S. Shen, *Energy*, 109 (2016) 620.
28. S. A. El-Khodary, I. S. Yahia, H.Y. Zahran and M. Ibrahim, *Physica B Condens. Matter.*, 556 (2019) 66.
29. N. A. Fathy, S. E. El-Shafey and O. I. El-Shafey, *J. Water Process Eng.*, 17 (2017) 95.
30. L. Chen, M. Zhang, X. Yang, W. Li, J. Zheng, W. Gan and J. Xu, *J. Alloys Compd.*, 695 (2017) 3339.
31. R. Kotz, and M. Carlen, *Electrochim. Acta*, 45 (2000) 2483.
32. D. Z. W. Tan, H. Cheng, S. T. Nguyen and H. M. Duong, *Mater. Technol. Adv. Func. Mater.,* 29 (2014) A2.
33. J. G. Wang, Y. Yang, Z. H. Huang, F. Kang, *Electrochim. Acta*, 75 (2012) 213.
34. F. Teng, S. Santhanagopalan, D. D. Meng, *Solid State Sci.*, 12 (2010) 1677.